HHS Public Access

Author manuscript

Lasers Surg Med. Author manuscript; available in PMC 2016 February 28.

Published in final edited form as:

Lasers Surg Med. 2016 February ; 48(2): 133–139. doi:10.1002/lsm.22415.

Confocal Imaging of Carbon Dioxide Laser-Ablated Basal Cell Carcinomas: An Ex-vivo Study on the Uptake of Contrast Agent and Ablation Parameters

Heidy Sierra, PhD[+], **Shadi Damanpour, BS**, **Brian Hibler, BS**, **Kishwer Nehal, MD**, **Anthony Rossi, MD**[*], and **Milind Rajadhyaksha, PhD**[*]

Dermatology Service, Memorial Sloan Kettering Cancer Center (HS, BPH, KSN, AMR, MR), 16 E. 60th Street, 4th Floor, New York, NY 10022. University of Miami Miller School of Medicine (SD), Miami, FL 33136

INTRODUCTION

Approximately 3.5 million new cases of non-melanoma skin cancers are diagnosed yearly in the United States, of which approximately 80% are basal cell carcinomas (BCCs) [1–2]. Mohs micrographic surgery, which relies on complete histopathological margin assessment, is the most common treatment for high-risk BCCs and provides highest cure rates (five-year, 97–99%) [3–4]. However, for less aggressive and low-risk subtypes of BCCs (i.e. superficial and early nodular), alternative treatment modalities can be less invasive, faster and lower-cost. These include electrodessication and curettage, topical chemotherapy (e.g. Imiquimod), cryotherapy, and coagulative and ablative laser therapies [5–8].

Laser ablation offers highly localized and precisely controlled removal of tissue, and can be particularly effective for minimally invasive treatment of superficial and early nodular BCCs [9–14]. To select the fluence and number of passes (sets of pulses), clinicians usually rely on visual examination and/or the diagnosis of tumor subtype and depth provided by a biopsy and histology [12–14]. However, visual examination may miss subclinical extension of lateral margins, while histology does not often allow for estimation of complete lateral and deep margins across the entire tumor. Furthermore, clinicians heavily rely on the visual appearance of the tissue between passes to estimate whether the tumor has been totally removed. During clinical follow up, monitoring the efficacy of the treatment is also typically based on visual observation. For all these reasons, there is high variability of recurrence rates, ranging from 3.23% to 50% [12–14]. Given the absence of definitive histological confirmation, there is a need for a non-invasive method to guide laser ablation, particularly

[+]Corresponding Author: Heidy Sierra, Ph.D., 16 E. 60th Street, 4th Floor, New York, NY 10022, Telephone: 646-888-6033, Fax: 646-227-7274, sierragh@mskcc.org.

[*]These authors contributed equally as senior authors

Disclosure Statement: Dr. Milind Rajadhyaksha is a former employee and owns equity in Caliber Imaging and Diagnostics (formerly Lucid Inc.), the company that manufactures and sells the Vivascope confocal microscope. The Vivascope is the commercial version of an original laboratory prototype that he had developed at Massachusetts General Hospital, Harvard Medical School.

The other authors have no disclosures or conflicts of interest to report.

for accurate determination of lateral and deep tumor margins, selection of laser parameters, and assessment of ablated tissue to confirm clearance of the tumor.

Optical imaging is being investigated for its ability to noninvasively guide the detection of lateral and deep margins of tumor, pre-, during and post-ablation [15–17]. By using a contrast agent, high-resolution microscopic-level imaging of cellular and sub-cellular detail can be obtained in post-ablated tissue *in vivo*. This allows for the presence (or absence) of residual tumor to be detected in post-ablated tissue, providing histopathology-like control directly on the patient. However, this is possible only with a specific set of parameters (number of passes and delivered fluence) that allow for simultaneous removal of BCCs, while controlling of the amount of underlying thermal coagulation, such that cellular structures can be subsequently labeled with a contrast agent and imaged [15–16].

We previously reported the feasibility of reflectance confocal microscopy (RCM) imaging to guide Erbium-doped yttrium aluminum garnet (Er: YAG) laser ablation, in both bench-top studies and on a small number of patients [15–17]. The Er: YAG laser (wavelength 2900nm) allows for vaporization of very thin layers of tissue while producing only a thin underlying zone of thermal coagulation. Two contrast agents, acetic acid and aluminum chloride, were shown to label nuclei and enhance contrast of nuclear morphology [18–21]. From the results, RCM imaging appears to be capable of detecting residual BCCs in post-ablated tissue [16–17].

Our studies have now expanded to include the carbon dioxide (CO_2) laser. The CO_2 laser (wavelength 10600nm) offers relatively more aggressive vaporization, along with relatively deeper thermal coagulation compared to the Er: YAG laser, affording greater tissue destruction with fewer passes and producing hemostasis in the underlying microvasculature [22–24].

In this paper, we report an *ex vivo* bench-top study to determine a set of effective ablation parameters (fluence, number of passes) for a CO_2 laser. We further report the results of an assessment of the uptake of acetic acid for contrast and our ability to utilize RCM imaging in post-ablated tissue to evaluate for the presence or absence of residual BCC tumors.

3. MATERIALS AND METHODS

Collection and preparation of skin specimens

Under an IRB approved protocol, 72 discarded fresh normal skin specimens and frozen BCC tumor specimens from Mohs surgery were collected. The frozen specimens of BCCs were thawed. In preparation for imaging, specimens were immersed in 5% acetic acid for 30 seconds to enhance nuclear brightness (“acetowhitening”). More details on the use and mechanism of acetic acid as a contrast agent for brightening nuclear morphology can be found in our earlier papers [20–21].

Reflectance confocal microscopy imaging

Imaging was performed using a benchtop reflectance confocal microscope, with 830nm illumination and a 30X, 0.9 numerical aperture, water immersion objective lens. The optical

sectioning is ~2μm with lateral resolution of ~0.7μm. Each image displays 0.5mm×0.5mm field of view, and a matrix of 16×16 images were collected and displayed as mosaics to increase the field of view to 8mm × 8mm. Skin specimens were cut in 5mm^2 to 8mm^2 pieces and mounted in a customized tissue fixture (mount) for imaging. Further details on the microscope, imaging, and tissue fixturing are available in earlier papers [21].

Laser ablation

The ablation was performed with a pulsed CO_2 laser (Lumenis/Coherent UltraPulse 5000C, San Jose, CA), with pulse duration ranging from 0.01ms to 5ms, and uniform spot of 2.25 mm in diameter (as stated in the company's product specifications). Ablation of large areas (size from ~5mm^2 to ~28mm^2) were performed by using the UltraScan computer-driven pattern generator that allows scanning of the spot either with or without overlap. Beam overlapping is typically used to minimize any edge effects and perform uniform ablation of large areas or to increase the delivered fluence at the center of the ablated area in single pass. In our study, a 30% overlap during scanning was chosen to allow uniform ablation over the entire area of interest.

Fluence values from ~5 to 12.5J/cm^2 were used in this study. The ablation threshold for a CO_2 laser is ~5.0/cm^2 which removes ~20–30μm of tissue, leaving an underlying thermal coagulation zone ranging from ~25μm to ~80μm thickness. For this study, we varied the fluence and number of passes, while keeping the pulse rate fixed (120 pulses/second). With a fixed pulse rate, as the fluence increases, the pulse duration increases. We ablated skin specimens at fluences of 5.5J/cm^2, 6.5J/cm^2, 7.5J/cm^2 and 8.5J/cm^2 (corresponding pulse duration of 724μs, 865μs, 947μs, and 1157μs, respectively) for 1 to 3 passes. This range of fluences is clinically relevant for the treatment of superficial and early nodular BCCs. Two specimens were ablated for each combination of parameters.

Evaluation of the effect of fluence on depth of ablation

To characterize the effect of fluence on the depth of ablation, we ablated normal skin specimens with intact stratum corneum. Ablating through intact stratum corneum simulates the conditions on patients *in vivo*. Two specimens were ablated at each fluence (mentioned above) and for each of 1–3 passes. The tissue was swabbed with saline-soaked gauze between passes to remove necrotic debris, following the standard approach on patients. Afterwards, vertical (oriented perpendicular to the tissue surface) hematoxylin and eosin (H&E)-stained sections were prepared to characterize the depth of ablation. Two measurements were made: one at the shallowest (edge) location and another at the deepest (center) of the ablated region relative to the adjacent non-ablated skin.

Evaluation of the uptake of contrast agent and imaging quality

Testing was first performed in normal skin specimens with intact stratum corneum to inspect the uptake of acetic acid in partially-ablated epidermis and evaluate the quality of RCM images post-ablation. Pre-ablation, specimens were first immersed in acetic acid and imaged to visualize cellular structures. Ablation was performed with the above set of parameters (fluence and number of passes). For each set of ablation parameters, 1 to 3 samples were tested. Post-ablation specimens were again immersed in acetic acid and imaged. Following

the imaging, e*n face* H&E-stained sections of the post-ablation imaged surface were prepared to visually examine the appearance of nuclear and dermal morphology. The *en face* sections are oriented parallel to the tissue surface and thus allowed for reasonably direct comparison between the RCM mosaics and the histopathology. The process was then repeated with three frozen-thawed BCC specimens for each combination of fluence and number of passes.

4. RESULTS

Depth of ablation

In Figures 1(a)–(c) the depth of ablation (between green arrows) associated with 1–3 passes of 7.5J/cm^2 is shown, as an example. Qualitatively, we observed an increase in the depth of ablation with increase in fluence and/or increase in number of passes. Table 1 presents a quantitative summary of the range for depths of ablation with fluence and number of passes in normal discarded skin specimens.

Partial epidermal ablation (between 20 and 60μm) was achieved with 1 pass at all fluences (5.5 to 8.5 J/cm2) with and also with more passes at the lower fluences (2 passes with 5.5 J/cm^2 and 6.5 J/cm^2. The epidermis was further and mostly ablated with more passes, 3 passes with the same fluences (5.5 J/cm2 and 6.5J/cm^2. With further increase in both fluence and number of passes, the epidermis was completely ablated along with superficial layers in the underlying dermis. With 2 and 3 passes of 7.5J/cm^2 and also with 2 passes of 8.5J/cm^2 complete epidermal removal is achieved down into the papillary dermis. Finally, partial reticular dermis ablation (100–150 μm) was seen with 3 passes of 8.5J/cm^2.

The results show a linear increase in the depth of ablation as a function of fluence. This behavior is in agreement with the ablative depth models presented in the literature [24], which demonstrate that the depth of ablation is linearly related to fluence from 4.5 J/cm^2 to 18J/cm^2. In our results, the depth of ablation slowly increases for 2 and 3 passes of 7.5 J/cm^2 and 8.5 J/cm^2 (as predicted by theory [24]). Since the depth of thermal coagulation also increases with increase in number of passes (higher total delivered fluence) this behavior was also expected.

Table 1 presents the experimentally measured and theoretically calculated depths of ablation for our fluence values and number of passes. The calculated values were obtained using a blow-off model [24], which predicts that $Depth\ of\ ablation = n \times [(1/a) \times Ln(Fluence/Threshold\ Fluence)]$, where n (n= 5) is the number of pulses in each train of pulses (“superpulse”) and a is the absorption coefficient of skin (a = 500cm^{-1}).

The results show that the modeled depths of ablation are relatively lower for the lowest fluences and relatively higher for higher fluences when compared to the measurements. This could be due to the assumption of a constant absorption coefficient for all the layers of skin. However, the stratum corneum and granular layers in the upper epidermis are relatively less hydrated (i. e., actual absorption coefficient may be lower than assumed), which may lead to an underestimation of the depth of ablation. In addition, the accumulative thermal coagulation for higher number of passes and higher fluences produces dehydration and

temperature changes in the confined volume of tissue during ablation which is known to decrease the ablation efficiency and reduce the depth of ablation. These factors may explain the differences between the modeled and actual numbers.

Uptake of contrast agent and imaging quality

For 1–3 passes of 5.5J/cm^2, 6.5J/cm^2, and 7.5J/cm^2 and 1–2 passes of 8.5J/cm^2, the ablated tissue retains the ability to uptake contrast agents to provide enhanced cellular-level morphologic detail on RCM imaging. For these fluences and number of passes, the depth of ablation is within ~125 μm. With these parameters, the appearance of nuclear patterns in normal structures (hair follicles, sebaceous glands, connective tissue and eccrine ducts) and the presence of residual tumor or clearance in surrounding dermis as observed in RCM images was confirmed with histopathology. The images were visually evaluated by Mohs surgeons and found to be of acceptable quality.

Figure 2 highlights the results for the labeling of nuclear morphology in post-ablated normal skin with two passes of 7.5 J/cm^2 as seen with RCM imaging (Figure 2(a)), and the agreement with the corresponding histology (Figure 2(b)). Figure 2(c) illustrates an enlarged view of the area enclosed in the yellow circle in Figure 2(a). The bright nuclei of basal cells in ring patterns (yellow arrows in Figure 2(c)) on dermal papillae in the exposed dermo-epidermal junction show the effect of acetowhitening in post-ablated tissue. Figure 2(d) shows details of these ring patterns in the corresponding histology.

In RCM images of post-ablated specimens containing tumor, nuclear morphology in residual BCC tumors appeared as densely clustered and bright nuclei, and the tumor-to-dermis contrast was enhanced by the effect of acetic acid. Figure 3(a) shows an example of a pre-ablation RCM mosaic from a specimen containing nodular BCC (bright areas or “nodules”). In Figure 3(d), an enlarged view of the red square in Figure 3(a), shows details of the tumor. Figure 3(b) and (c) show an RCM mosaic and histopathology images of the specimen, post-ablation after three passes of 7.5J/cm^2. The enlarged view of the tumor post-ablation seen in Fig. 3(e) showing clusters of bright nuclei corresponds to presence of residual tumor (yellow arrows). Also, seen in surrounding areas is clearance of tumor (dashed green arrows) confirmed with histopathology (Figure 3(f)).

In summary, RCM images allow visualizing changes in the morphology of BCC tumors after CO_2 ablation, showing destruction as well as coagulation changes in the surrounding dermal stroma. For the parameters of our laser, the maximum total delivered fluence allowing for removal of BCC while maintaining contrast uptake and adequate RCM imaging quality was 22.5J/cm^2 (3 passes at 7.5J/cm^2) in any single treatment. We noted that beyond this fluence, such as ablation at 8.5J/cm^2 for 3 passes resulted in excessive distortion of tissue architecture, and did not allow for adequate uptake of the nuclear contrast agent and impaired imaging quality in both normal tissue and BCC-containing tissue. As such, while these more aggressive parameters may allow for quick and complete tumor destruction, they will not permit for post-ablation tissue imaging with RCM to evaluate for presence or clearance of residual tumor.

5. DISCUSSION

Laser ablation continues to be of interest as a potentially less invasive alternative to traditional Mohs surgery for the treatment of low-risk superficial and nodular subtypes of BCCs. Precise, rapid, and highly localized tissue vaporization can be achieved with ablative Er: YAG and CO_2 lasers. Studies have also reported that both lasers can provide similar depth of ablation, depth of thermal coagulation, and cosmetic outcomes by varying pulse duration, fluence, and number of passes [22–23]. However, a limitation of laser ablation for treating skin cancers has been the inability to confirm clearance of tumor without the availability of subsequent pathology, as is routinely performed to guide Mohs surgery and surgical excision. Our imaging studies intend to address this limitation.

As a first step, we have shown that clinically acceptable-quality RCM imaging is possible with adequate optical sectioning, resolution and clear appearance of nuclear and BCC tumor morphology in post-ablated skin tissue. The results of this bench-top ex vivo study suggest that a range of ablation parameters may be used to control the underlying coagulation, which then allows uptake of contrast agent and the use of RCM imaging to detect the presence (or absence) of residual BCC tumor. The imaging may also allow accurate selection of the CO_2 laser parameters for precise ablation down to a specified depth, permitting destruction of the tumor while sparing as much normal tissue as possible.

A possible limitation may be the reliance on reflectance for contrast. Acetic acid as a contrast agent has shown promising results to detect large (larger than ~100μm) BCC tumors. However, due to the brightness of the surrounding dermal tissue, the detection of small tumors could be a challenge. The use of either endogenous autofluorescence contrast or exogenous contrast agents (methylene blue, fluorescein, Rose Bengal) and imaging in fluorescence may address this limitation. With fluorescence, the dermis will be relatively darker and the tumor to dermal contrast is likely to be relatively stronger. Further studies on the development and use of an appropriate contrast agent is warranted, including testing for accuracy of imaging in terms of, particularly, specificity and negative predictive value.

Another limitation is that this ex vivo study could not account for the influence of tissue temperature and blood flow. The study demonstrated that using total delivered fluence of more than 22.5J/cm^2 impaired the uptake of acetic acid and subsequent imaging quality, making it difficult to effectively interpret RCM images and detect cutaneous architecture. This could be due to increased coagulation in the confined volume of relatively small tissue specimens due to lack of cooling and/or variability of the tissue (size, thickness), both of which were not controlled for the purpose of this study. More studies are necessary, on the impact of tissue volume and variability, active cooling of tissue between passes and resulting thermal coagulation zone on the uptake of contrast agent and image quality in post-ablated tissue. These two factors will influence the outcome in patients, and will be warranted in follow-up clinical studies.

Our results, although preliminary and with some limitations, are nonetheless encouraging for the eventual possibility of RCM imaging-guided laser ablation of superficial and nodular BCCs on patients. In parallel with the ongoing ex vivo study, we have initiated a small pre-

clinical in vivo feasibility study to test the ablation parameters and RCM imaging. The preliminary results in ten patients have shown that the uptake of contrast agent and imaging quality in vivo is feasible, similar to that observed in the ex vivo study presented here. Long-term clinical studies will be the next phase of this effort, to evaluate the accuracy of imaging (particularly, specificity and negative predictive value), recurrence rates, cosmetic benefits, and cost-to-benefits relative to traditional surgical approaches (Mohs surgery, surgical excision). Methods and guidelines to read and interpret RCM images of post-ablated presence or clearance of residual BCCs will be necessary, as well, similar to the training currently in progress for RCM imaging-guided diagnosis of non-melanoma skin cancers [25–26]. Finally, in the longer-term, our studies may offer a basis for RCM imaging to guide other treatment modalities, which are also being developed, such as topical Imiquimod therapy and photodynamic therapy [27–28] for treatment of BCCs and laser treatment of superficial skin disorders [29–30].

Acknowledgments

Funding Sources: This work was supported by a National Institute of Health grant, R01EB012466, from the National Institute of Biomedical Imaging and Bioengineering Image-guided Interventions program.

Brian Hibler was a recipient of the ASLMS travel grant for work related to this project.

We thank the NIH for funding support (grant R01EB012466 from NIBIB's Image-guided Interventions program) as well William Phillips and Marie Tudisco for their help with preparation of histology sections.

References

1. Lomas A, Leonardi-Bee J, Bath-Hextall F. A systematic review of worldwide incidence of nonmelanoma skin cance. Br J Dermatol. 2012; 166(5):1069–80. [PubMed: 22251204]
2. Berking C, Hauschild A, Kölbl O, Mast G, Gutzmer R. Basal cell carcinoma-treatments for the commonest skin cancer. Dtsch Arztebl Int. 2014; 111(22):389–95. [PubMed: 24980564]
3. Mohs FE. Chemosurgery - a microscopically controlled method of cancer excision. Arch Surg. 1941; 42:279–295.
4. Chren MM, Linos E, Torres JS, Stuart SE, Parvataneni R, Boscardin WJ. Tumor recurrence 5 years after treatment of cutaneous basal cell carcinoma and squamous cell carcinoma. J Invest Dermatol. 2013; 133(5):1188–96. [PubMed: 23190903]
5. Amini S, Viera MH, Valins W, Berman B. Nonsurgical Innovations in the Treatment of Nonmelanoma Skin Cancer. J Clin Aesthet Dermatol. 2010; 3(6):20–34.
6. Konnikov N, Avram M, Jarell A, Tannous Z. Pulsed Dye Laser as a Novel Non-Surgical Treatment forBasal Cell Carcinomas: Response and Follow Up 12–21 Months After Treatment. Lasers in Surgery and Medicine. 2011; 43:72–78. [PubMed: 21384387]
7. Ibrahimi OA, Sakamoto FH, Tannous Z, Anderson RR. 755nm Alexandrite Laser for the Reduction of Tumor Burden in Basal Cell Nevus Syndrome. Lasers Surg Med. 2011; 43(2):68–71. [PubMed: 21384386]
8. Jalian HR, Avram MM, Stankiewicz KJ, Shofner JD, Tannous Z. Combined 585 nm pulsed-dye and 1,064 nm Nd:YAG lasers for the treatment of basal cell carcinoma. Lasers Surg Med. 2014; 46(1): 1–7. [PubMed: 24272664]
9. Nouri K, Chang A, Trent JT, Jiménez GP. Ultrapulse CO_2 used for the successful treatment of basal cell carcinomas found in patients with basal cell nevus syndrome. Dermatol Surg. 2002; 28(3):287–90. [PubMed: 11896785]
10. Humphreys TR, Malhotra R, Scharf MJ, Marcus SM, Starkus L, Calegari K. Treatment of superficial basal cell carcinoma and squamous cell carcinoma in situ with a high- energy pulsed carbon dioxide laser. Arch Dermatol. 1998; 134:1247–1252. [PubMed: 9801680]

11. Ebrahimi A, Rezaei M, Kavoussi R, Eidizadeh M, Hamid Madani S, Kavoussi H. Superpulsed CO_2 Laser with Intraoperative Pathologic Assessment for Treatment of Periorbital Basal Cell Carcinoma Involving Eyelash Line. Dermatology Research and Practice. 2014; 201410.1155/2014/931657
12. Kavoussi H, Ebrahimi A. Treatment and cosmetic outcome of superpulsed CO_2 laser for basal cell carcinoma. Acta Dermatovenerol Alp Pannonica Adriat. 2013; 22(3):57–61. [PubMed: 24089133]
13. Del Pozo J, Rosende L. Basal Cell Carcinoma. Treatment with Carbon Dioxide Laser Vaporization. Advances in Cancer Research & Treatment. 2013; 201310.5171/2013.442049
14. Iyer S, Bowes L, Kricorian G, Friedli A, Fitzpatrick RE. Treatment of basal cell carcinoma with the pulsed carbon dioxide laser: a retrospective analysis. Dermatol Surg. 2014; 30(9):1214–8. [PubMed: 15355363]
15. Chen CS, Sierra H, Cordova M, Rajadhyaksha M. Confocal microscopy-guided laser ablation for superficial and early nodular Basal cell carcinoma: a promising surgical alternative for superficial skin cancers. JAMA Dermatololgy. 2014; 150(9):994–8.
16. Sierra H, Larson BA, Chen CS, Rajadhyaksha M. Confocal microscopy to guide erbium:yttrium aluminum garnet laser ablation of basal cell carcinoma: an ex vivo feasibility study. J Biomed Opt. 2013; 18(9):095001. [PubMed: 24045654]
17. Sierra H, Chen J, Cordova M, Rajadhyaksha M. Confocal imaging-guided laser ablation of basal cell carcinomas: an ex vivo study. J of Invest Dermatol. 2014; 135:612–615. [PubMed: 25178106]
18. Tannous Z, Torres A, González S. In vivo real-time confocal reflectance microscopy: a noninvasive guide for Mohs micrographic surgery facilitated by aluminum chloride, an excellent contrast enhancer. Dermatol Surg. 2003; 29:839–46. [PubMed: 12859385]
19. Scope A, Mahmood U, Gareau DS, Kenkre MM, Lieb J, Nehal KS, Rajadhyaksha M. In vivo reflectance confocal microscopy of shave biopsy wounds: feasibility of intra-operative mapping of cancer margins. Br J Dermatol. 2010; 163(6):1218–1228. [PubMed: 20874785]
20. Patel YG, Nehal KS, Aranda I, Li Y, Halpern AC, Rajadhyaksha M. Confocal reflectance mosaicing of basal cell carcinomas in Mohs surgical skin excisions. J Biomedical Optics. 2007; 12(3):034027. [PubMed: 17614735]
21. Gareau DS, Patel YG, Li Y, Aranda I, Halpern AC, Nehal KS, Rajadhyaksha M. Confocal mosaicing microscopy in skin excisions: a demonstration of rapid surgical pathology. J Microscopy. 2009a; 233:149–159.
22. Goldman, MP.; Roston, E. Combined Laser Resurfacing Techniques. In: Kauvar, ANB.; Hruza, GJ., editors. Principles and Practices in Coetaneous Laser Surgery. Taylor & Francis Group; 2005. p. 569-589.
23. Tanzi EL, Alster TS. Single-Pass Carbon Dioxide Versus Multiple-Pass Er:YAG Laser Skin Resurfacing: A Comparison of Postoperative Wound Healing and Side-Effect Rates. Dermatologic Surgery. 2003; 29(1):80–84. [PubMed: 12534517]
24. Walsh JT, Deutsch TF. Pulsed CO2 laser tissue ablation: measurement of the ablation rate. Lasers Surg Med. 1988; 8(3):264–75. [PubMed: 3134586]
25. Scope A, Benvenuto-Andrade C, Agero AL, Malvehy J, Puig S, Rajadhyaksha M, Busam KJ, Marra DE, Torres A, Propperova I, Langley RG, Marghoob AA, Pellacani G, Seidenari S, Halpern AC, Gonzalez S. In vivo reflectance confocal microscopy imaging of melanocytic skin lesions: consensus terminology glossary and illustrative images. J Am Acad Dermatol. 2007 Oct; 57(4): 644–58. Epub 2007 Jul 16. [PubMed: 17630045]
26. Gonzalez, SG.; Gill, M.; Halpern, AC., editors. Reflectance Confocal Microscopy of Cutaneous Tumors – An Atlas with Clinical, Dermoscopic and Histological Correlations. Informa Healthcare; London: 2008. p. 60-89.
27. Ulrich M, Lange-Asschenfeldt S, Gonzalez S. The use of reflectance confocal microscopy for monitoring response to therapy of skin malignancies. Dermatol Pract Concept. 2012; 2(2):43–52.
28. Venturini M, Sala R, Gonzàlez S, Calzavara-Pinton PG. Reflectance confocal microscopy allows in vivo real-time noninvasive assessment of the outcome of methyl aminolaevulinate photodynamic therapy of basal cell carcinoma. Br J Dermatol. 2013 Jan; 168(1):99–105.10.1111/bjd.12052 [PubMed: 23013443]

29. Longo C, Pellacani G, Tourlaki A, Galimberti M, Bencini PL. Melasma and low-energy Q-switched laser: treatment assessment by means of in vivo confocal microscopy. Lasers Med Sci. 2014; 29(3):1159–63. [PubMed: 24292199]

30. Richtig E, Hofmann-Wellenhof R, Kopera D, El-Shabrawi-Caelen L, Ahlgrimm-Siess V. In vivo analysis of solar lentigines by reflectance confocal microscopy before and after Q-switched ruby laser treatment. Acta Derm Venereol. 2011 Mar; 91(2):164–8. [PubMed: 21246177]

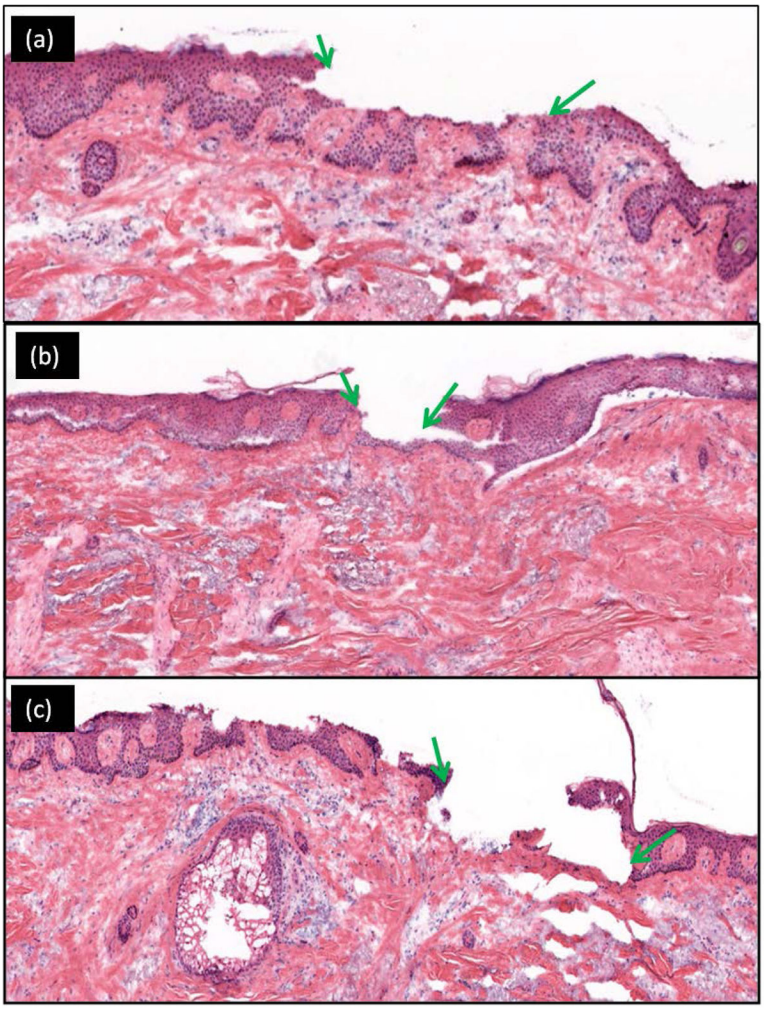

Figure 1.

Increasing depth of ablation is seen with increasing number of passes. The post-ablated region (between green arrows) is seen on vertical histology after tissue ablation with a fluence of 7.5 J/cm^2. For this specimen (a) 1 pass, removed ~30 – 55 um (partial epidermis); (b) 2 passes, ~60 – 80 um (complete epidermis to papillary dermis); and (c) 3 passes, ~90 – 110 um (complete epidermis to reticular dermis).

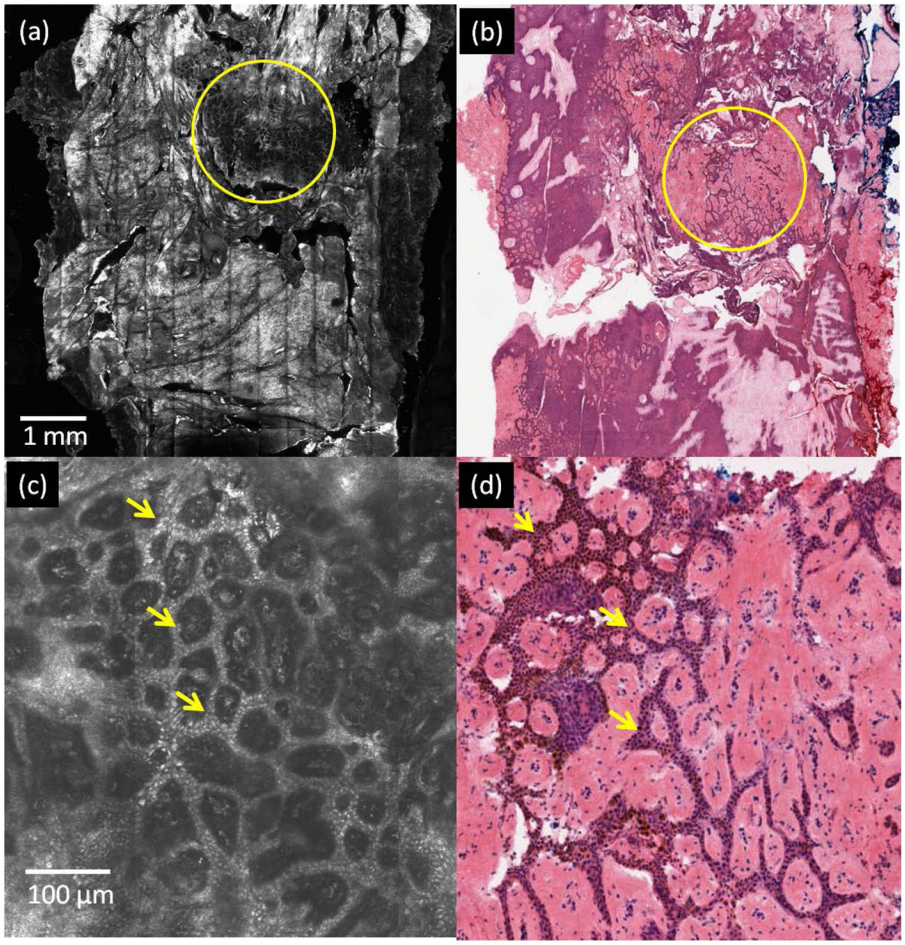

Figure 2.

Labeling of nuclear morphology in post-ablated normal skin tissue. Bright nuclei, labeled with acetic acid, are seen at the dermoepidermal junction in a specimen ablated with two passes of 7.5 J/cm^2. (a) RCM mosaic of specimen with partially ablated epidermis (region enclosed in yellow circle), (b) corresponding *en face* histology, (c) enlarged view of the yellow circled ablated region in (a) shows bright nuclei (yellow arrows) in basal cells, arranged in ring patterns on dermal papillae (d) corresponding area on histology, showing purple-stained nuclei in similar ring patterns.

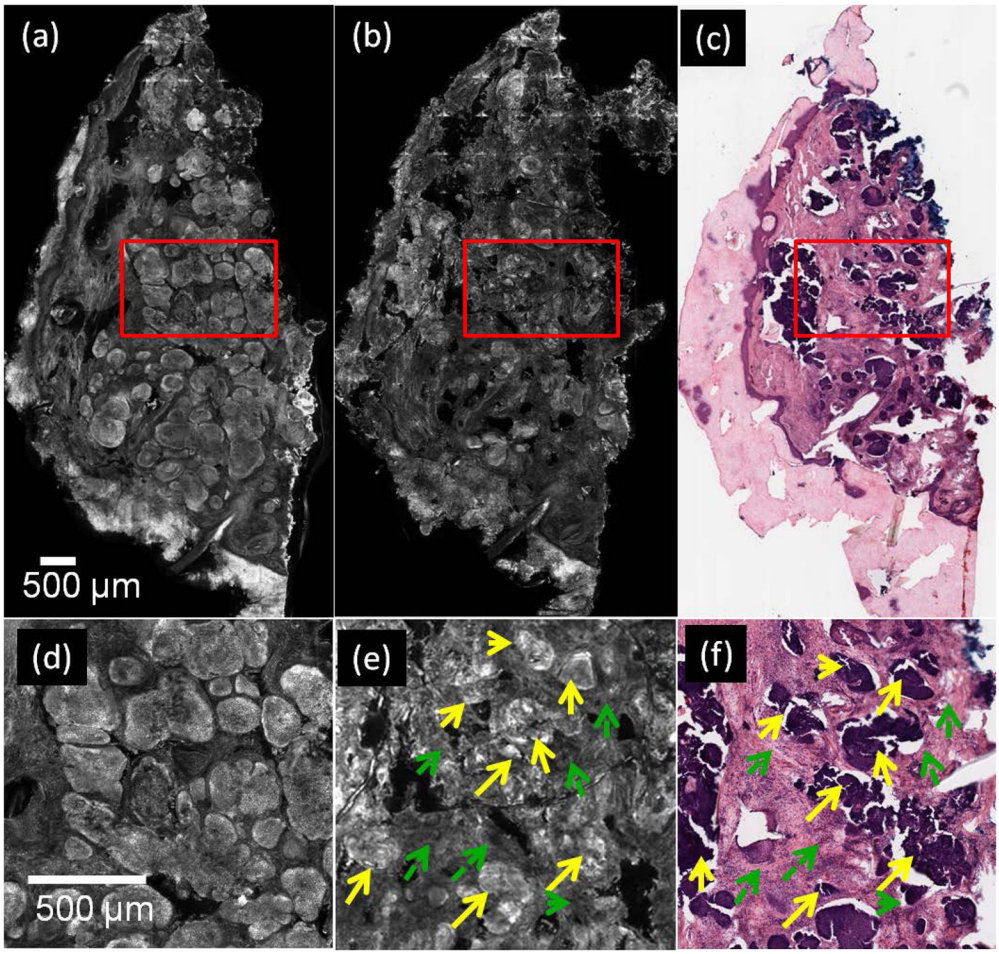

Figure 3.

Nuclei are labeled with acetic acid in BCC tumors, after ablation with three passes at 7.5 J/cm^2. (a) pre-ablation RCM mosaic of specimen containing nodular BCCs (bright regions or “nodules”), (b) RCM mosaic of post-ablated specimen, (c) corresponding post-ablation *en face* histology, (d) and (e) are enlarged views of the red square regions in (a) and (b), respectively, showing bright nuclei in areas containing tumor, pre-ablation (d) and post-ablation (solid yellow arrows) (e), darker appearing surrounding normal dermis (dashed-green arrows), (f) enlarged view of red square in (c) showing the same region as seen in (e). Purple stained nuclei (yellow arrows) and pink stained dermis (green arrows) are seen.

Table 1

Tissue removal (depth of ablation) in normal skin specimens.

Fluence (J/cm^2)	1 pass		2 passes		3 passes	
	Model	**Measured**	**Model**	**Measured**	**Model**	**Measured**
5.5	20 μm	~20 to 30 μm (partial epidermis)	40 μm	~40 to 55 μm (partial epidermis)	60 μm	~60 to 75 μm (most of the epidermis)
6.5	37 μm	~20 to 40 μm (partial epidermis)	74 μm	~40 to 60μm (partial epidermis)	110 μm	~60 to 85 μm (most of the epidermis)
7.5	51 μm	~30 to 45um (partial epidermis)	102 μm	~70 to 110um (complete epidermis to papillary dermis)	153 μm	~80 to 125um (complete epidermis to papillary dermis)
8.5	63 μm	~35 to 50 um (partial epidermis)	127 μm	~90 to 115um (complete epidermis to papillary dermis)	190 μm	~100 to 150 μm (Papillary dermis to partial reticular dermis)